

RHL1 is an essential component of the plant DNA topoisomerase VI complex and is required for ploidy-dependent cell growth

Keiko Sugimoto-Shirasu^{*†‡}, Gethin R. Roberts[†], Nicola J. Stacey^{*}, Maureen C. McCann^{*§}, Anthony Maxwell[†], and Keith Roberts^{*}

Departments of ^{*}Cell and Developmental Biology and [†]Biological Chemistry, John Innes Centre, Colney, Norwich NR4 7UH, United Kingdom

Edited by Marc C. E. Van Montagu, Ghent University, Ghent, Belgium, and approved October 17, 2005 (received for review July 13, 2005)

How cells achieve their final sizes is a pervasive biological question. One strategy to increase cell size is for the cell to amplify its chromosomal DNA content through endoreduplication cycles. Although endoreduplication is widespread in eukaryotes, we know very little about its molecular mechanisms. Successful progression of the endoreduplication cycle in *Arabidopsis* requires a plant homologue of archaeal DNA topoisomerase (topo) VI. To further understand how DNA is endoreduplicated and how this process is regulated, we isolated a dwarf *Arabidopsis* mutant, *hyp7* (*hypocotyl 7*), in which various large cell types that in the wild type normally endoreduplicate multiple times complete only the first two rounds of endoreduplication and stall at 8C. *HYP7* encodes the RHL1 (ROOT HAIRLESS 1) protein, and sequence analysis reveals that RHL1 has similarity to the C-terminal domain of mammalian DNA topo II α , another type II topo that shares little sequence homology with topo VI. RHL1 shows DNA binding activity *in vitro*, and we present both genetic and *in vivo* evidence that RHL1 forms a multiprotein complex with plant topo VI. We propose that RHL1 plays an essential role in the topo VI complex to modulate its function and that the two distantly related topoisomerases, topo II and topo VI, have evolved a common domain that extends their function. Our data suggest that plant topo II and topo VI play distinct but overlapping roles during the mitotic cell cycle and endoreduplication cycle.

endoreduplication | hypocotyl | root hairless

The control of cell size is a highly regulated process with inputs from genetic, hormonal, and environmental cues. Yeast and mammalian cells usually only double their size during their development; therefore, a key question in their size control is how proliferating cells coordinate cell growth and cell division to maintain size homeostasis. Yeast and many mammalian cells have a cell size checkpoint mechanism in which cells divide only when they reach a critical size (1), whereas some mammalian cells may control their size through extracellular signals (2). Although plant cells also double their cell size during proliferation, they commonly undergo an additional, massive (sometimes >1,000-fold), postmitotic cell enlargement. Such a large increase in volume is driven by a combination of production of new cytoplasmic mass and cell expansion (driven by water uptake and vacuolar growth), but little is known about the underlying mechanisms involved. Recent genetic evidence strongly supports the classical “karyoplasmic ratio” theory that one mechanism to increase cell size is by increasing the ploidy level within a cell, for example through endoreduplication, defined as the amplification of chromosomal DNA without corresponding cell division (3). Several mutants and transgenic plants that have aberrant levels of endoreduplication have been isolated and have led to the identification of key regulators of the endoreduplication cycle or endocycle (3–7). How these regulators control downstream events, however, remains to be elucidated.

Mutations in the plant homologue of an archaeal DNA topoisomerase (topo) VI result in an extreme dwarf phenotype (8–10).

topo VI is a heterotetrameric A₂B₂ enzyme that forms a subclass of type II topo (type IIB) and is thought to decatenate replicated chromosomes in archaea (11). Unlike wild-type seedlings, in which some large cell types undergo up to four rounds of endoreduplication and reach 32C (C = haploid DNA content), mutants in topo VI subunits A and B, *rhl2* (*root hairless 2*) and *hyp6* (*hypocotyl 6*), respectively, progress through only the first two endocycles and stall at 8C, suggesting that topo VI is required to resolve intertwined and entangled chromosomes during endocycles above 8C (9, 10). As part of our investigation of the molecular mechanism of endoreduplication and cell size control in plants, we isolated a mutant, *hyp7*, from a mutant screen for dark-grown short-hypocotyl phenotypes. In this manuscript, we show that *HYP7* encodes the RHL1 protein that has DNA-binding activity and provide evidence that RHL1 plays an essential role in successive endocycles as a component of the plant topo VI complex.

Materials and Methods

Plant Material and Growth Conditions. The *hyp7* mutant was isolated from a screen of short-hypocotyl mutants. The *rhl1-1*, *rhl2-1*, and *rhl3-1* mutants were isolated previously (9, 12). The *kak2* (*kaktus 2*), *rfl* (*rastafari*), and *try* (*triptychon*) mutants (13) were provided by Martin Hulskamp (University of Cologne, Cologne, Germany). Plants were grown on plates containing MS salts (pH 5.8), 1% (wt/vol) sucrose, and 0.5% (wt/vol) phytigel. Callus was produced from wild-type and *hyp7* roots dissected from 7-day-old seedlings and grown on plates as described by May and Leaver (14).

Histochemical Analysis of β -Glucuronidase (GUS). The *GL2::GUS* reporter construct (15) was introduced into *hyp7* by a genetic cross. Seedlings were fixed in 90% acetone at -20°C for 1 h and incubated in GUS staining buffer (100 mM NaH₂PO₄/10 mM Na₂EDTA/0.5 mM K₃Fe(CN)₆/0.5 mM K₄Fe(CN)₆·3H₂O/0.1% Triton X-100/0.5 mg/ml X-glucuronide, pH 7.0) for 1 h.

Ploidy Measurements. The ploidy level of 14-day-old leaf nuclei was measured by flow cytometry as described in ref. 9. To examine the ploidy level of trichome and root hair cells, 14-day-old seedlings were fixed in 3:1 95% ethanol/acetic acid, cleared in 100% ethanol, and rehydrated through an ethanol series (90%, 70%, 50%, and 30%). Leaves were stained with Cystain fluorescent buffer (Partec, Münster, Germany) and washed three times in water. Nuclear images were recorded by epifluorescence microscopy (model E600, Nikon). The ploidy level was measured by using the area and mean

Conflict of interest statement: No conflicts declared.

This paper was submitted directly (Track II) to the PNAS office.

Freely available online through the PNAS open access option.

Abbreviations: topo, topoisomerase; GUS, β -glucuronidase;

[†]To whom correspondence should be addressed. E-mail: keiko.sugimoto@bbsrc.ac.uk.

[§]Present address: Department of Biological Sciences, Purdue University, West Lafayette, IN 47907-1392.

© 2005 by The National Academy of Sciences of the USA

gray value tool of IMAGEJ 1.32j (16) and was expressed as area \times mean gray value.

Yeast Two-Hybrid Assay. Full-length cDNAs of *RHL1*, *RHL1^{rh1-2}*, *AtSPO11-3/RHL2*, and *AtTOP6B/HYP6/RHL3* were amplified from RT-PCR products and cloned into pLexA (binding-domain fusion) or pB42AD (activator-domain fusion) vectors (Matchmaker LexA two-hybrid system, Clontech). Interactions were detected by the induction of the *lacZ* reporter genes under the control of the *lexA* gene in yeast EGY48 cells.

Semiquantitative RT-PCR and *in Vivo* Localization Analysis. For semiquantitative RT-PCR, total RNAs were extracted from leaves by using an RNeasy kit (Qiagen, Valencia, CA) and treated with RNase-free DNase I (Roche). One microgram of DNA-free total RNA was reverse-transcribed with Expand reverse transcriptase (Roche). For cell cycle transition studies, 9-, 15-, 22-day-old leaves were prepared according to Beemster *et al.* (17).

To study the *in vivo* expression pattern of plant topo VI proteins, a 3-kb genomic fragment of *AtSPO11-3/RHL2* that comprises its 1.5-kb 5' upstream region and 1.5-kb coding sequence were PCR-amplified and subcloned as a KpnI-XhoI fragment into the pGR4 vector, which contains a C-terminal GFP tag. The resultant *pRHL2::RHL2::GFP* was transformed into wild-type *Arabidopsis* seedlings by an *Agrobacterium*-mediated transformation method (18).

GFP images were recorded by using epifluorescence microscopy (Nikon E600, Japan) equipped with a cooled charge-coupled device digital camera (Hamamatsu, Hamamatsu City, Japan). Three-dimensional images were obtained by collecting 10–15 optical sections (each section $\approx 1 \mu\text{m}$ thick) in the *z* axis. *Z* sections were deconvolved with AutoDeblur (AutoQuant, Troy, NY) and projected with IMAGEJ.

Results

***hyp7* Has a Reduced Cell Size Phenotype.** The *hyp7* mutant exhibits an extreme dwarf phenotype similar to that of *rh12* and *hyp6* (9) in the dark and in the light (Fig. 1*A–D*). Scanning electron microscopy revealed that the leaf adaxial epidermis of *hyp7* lacks the large interlocked pavement cells characteristic of wild-type leaves (Fig. 1*I*) and that the epidermal cells develop as small, smooth-surfaced cells (Fig. 1*J*). By quantifying the surface area of these epidermal cell types, we found that the maximum cell size in *hyp7* is reduced at least to half that of the wild type (Fig. 6, which is published as supporting information on the PNAS web site). The size of the trichomes, another large cell type in the leaf epidermis, is also reduced in *hyp7* and is accompanied by reduced branching (Fig. 1*K* and *L*). In contrast, guard cells in *hyp7* appear to be normal in size and shape (Fig. 1*I* and *J*), and, although the total number of adaxial epidermal cells in an individual *hyp7* leaf is reduced by ≈ 2 -fold, the frequency and patterning of trichomes and guard cells do not appear to be affected (data not shown). The growth of root hairs is also severely disturbed in *hyp7*, with only a few visible hairs on primary roots (Fig. 1*M* and *N*). We tested whether *hyp7* has defects in cell proliferation by dissecting root segments from 7-day-old seedlings and inducing callus formation on culture plates. As shown in Fig. 1*O* and *P*, *hyp7* calli can grow for 4–6 weeks with a growth rate similar to wild-type calli. In addition, we found that cells in wild-type and *hyp7* calli are within a similar size range (Fig. 1*Q* and *R*), suggesting that *hyp7* calli contain a similar number of cells and, thus, that *hyp7* cells can proliferate mitotically as efficiently as wild-type cells.

Lack of fully developed trichomes and root hairs in *hyp7* could result from impairment in either the initial cell fate specification or subsequent cell enlargement. To test whether trichomes and root hairs in *hyp7* have their cell fates correctly specified, we introduced a *GL2::GUS* construct (15) into *hyp7* to mark the differentiation of trichomes and root hairs. The *GL2* gene is expressed preferentially

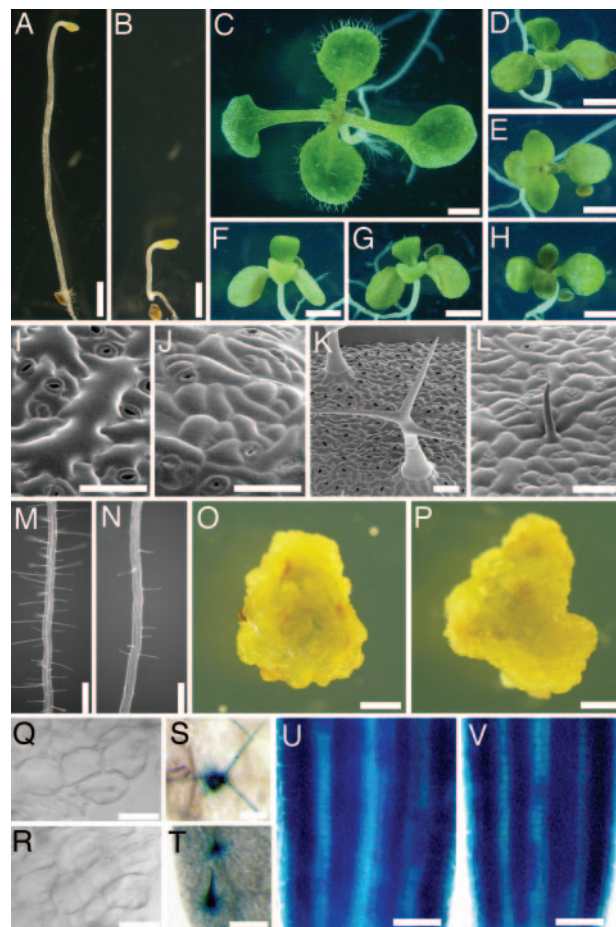


Fig. 1. Dwarf and compromised cell size phenotypes of *hyp7*. (*A* and *B*) One-week-old, dark-grown seedlings. (*C–H*) Two-week-old, light-grown seedlings. (*I* and *J*) Scanning electron micrographs of fully expanded, leaf adaxial epidermal cells from 14-day-old seedlings. (*K* and *L*) Scanning electron micrographs of fully mature trichomes. (*M* and *N*) Seven-day-old roots. (*O* and *P*) Four-week-old callus induced from roots. (*Q* and *R*) Cells from 4-week-old callus. (*S* and *T*) *GL2::GUS* expression in leaf epidermis. (*U* and *V*) *GL2::GUS* expression in root epidermis. (*A*, *C*, *I*, *K*, *M*, *O*, *Q*, *S*, and *U*) Wild-type Columbia ecotype. (*B*, *D*, *J*, *L*, *N*, *P*, *R*, *T*, and *V*) *hyp7*. (*E*) *rh13-1*. (*F*) *rh12-1*. (*G*) *hyp7 rh12-1*. (*H*) *hyp7 rh13-1*. (Scale bars: 2 mm in *A–H*, *O*, and *P*; 50 μm in *I–L*, *U*, and *V*; 100 μm in *M*, *N*, *S*, and *T*; and 25 μm in *Q* and *R*.)

in trichomes in wild-type leaves (Fig. 1*S*) and non-hair-forming cell files (atrachoblasts) in wild-type roots (Fig. 1*U*). We found that *hyp7* has similar *GL2::GUS* expression patterns in leaf trichomes (Fig. 1*T*) and in root atrichoblasts (Fig. 1*V*), suggesting that trichomes and root hairs in *hyp7* have been correctly specified but subsequently fail to increase in size.

HYP7 Is Essential for Successive Endocycles Beyond 8C. The growth defects of *hyp7* in cell types that normally endoreduplicate, i.e., hypocotyl cells, leaf pavement cells, trichomes, and root hairs, suggest that *hyp7* has a ploidy defect. Flow cytometric analysis revealed that cells in 14-day-old wild-type *Arabidopsis* leaves endoreduplicate up to four times to reach 32C, but *hyp7* goes through only two endocycles and halts at 8C (Fig. 2*A* and *B*). In addition, by quantifying the size of DAPI-labeled nuclei relative to the nuclei in guard cells (Fig. 2*E*) and root cap cells (Fig. 2*H*) as 2C controls, we found that fully differentiated wild-type trichomes and root hair cells contain nuclei up to 32C ($n = 30$) and 16C ($n = 30$), respectively (Fig. 2*C* and *F*), but only up to 8C in *hyp7* ($n = 30$) (Fig. 2*D* and *G*). To further characterize the nature of the endoreduplication defect in *hyp7*, we generated double mutants between *hyp7*

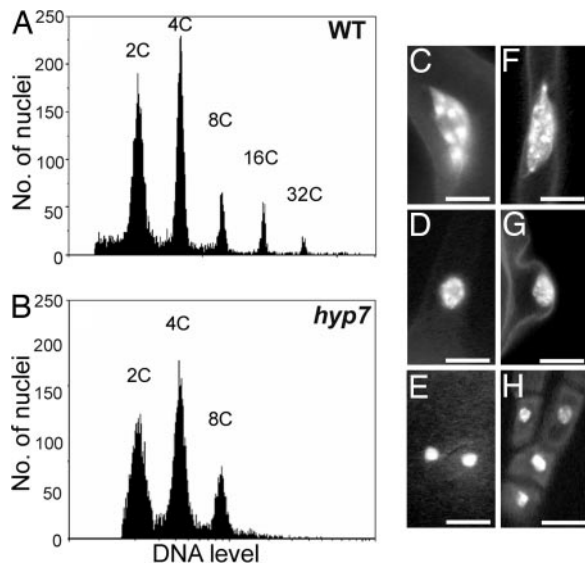


Fig. 2. Ploidy level is reduced in *hyp7*. (A and B) Flow cytometric analysis of 14-day-old leaves. (C–H) DAPI-stained nuclei in trichome cells (C and D) and root hair cells (F and G). (A, C, and F) Wild type. (B, D, and G) *hyp7*. (E and H) The nuclei in guard cells (E) and root cap cells (H) represent 2C. (Scale bars: 10 μ m.)

and several over-endoreduplicated, over-branched trichome mutants, such as *kak2*, *rfl*, and *try* (19). (For details, see *Supporting Materials and Methods*, which is published as supporting information on the PNAS web site.) As shown in Fig. 7, which is published as supporting information on the PNAS web site, *hyp7 kak2*, *hyp7 rfl*, and *hyp7 try* double mutants have small, under-branched trichomes similar to those found in *hyp7*, suggesting that *hyp7* is epistatic to *kak2*, *rfl*, and *try* for the trichome growth and branching phenotypes. In all double mutants, the maximum ploidy level remains at approximately 8C (data not shown). The plant hormone gibberellin promotes one extra endocycle and additional branching in wild-type *Arabidopsis* trichomes (19). However, the application of exogenous gibberellin to *hyp7* seedlings does not rescue the under-endoreduplicated, under-branched trichome phenotype (data not shown), suggesting that HYP7 is essential for successive endocycles beyond 8C.

Positional Cloning of HYP7 and RHL3. By positional cloning (see *Supporting Materials and Methods* for details), we found that HYP7 encodes the RHL1 protein (At1g48380) (20). The *hyp7* mutation substitutes adenine for guanine in the first exon and replaces the amino acid glycine (Gly-79) with aspartic acid (Fig. 3A, g→a). The previously described mutant allele *rhl1*, which has a T-DNA insertion in the first exon (20), has a dwarf and reduced ploidy phenotype indistinguishable from *hyp7* (data not shown), and F1 plants from crosses between *rhl1* and *hyp7* show the same mutant phenotype, thus confirming the identity of the gene. We therefore renamed *hyp7* as *rhl1-2*. RT-PCR analysis revealed that the *rhl1-2* mutation alters neither the size nor abundance of the RHL1 transcript (Fig. 3B). However, the mutation appears to destabilize the RHL1 protein because our immunoblot analysis with an RHL1-specific antiserum did not detect a corresponding protein band in *rhl1-2* (Fig. 3C).

Because *rhl1* and *rhl2* were originally isolated in a mutant screen (12) together with another similar mutant, *rhl3*, we reexamined this third mutant. Phenotypic and flow cytometric analyses revealed that *rhl3* exhibits almost the same phenotype as *rhl1* and *rhl2*, i.e., an extreme dwarf (Fig. 1E) associated with reduced cell size and ploidy level (data not shown). By using positional cloning, we found that RHL3 is allelic to *AtTOP6B*/

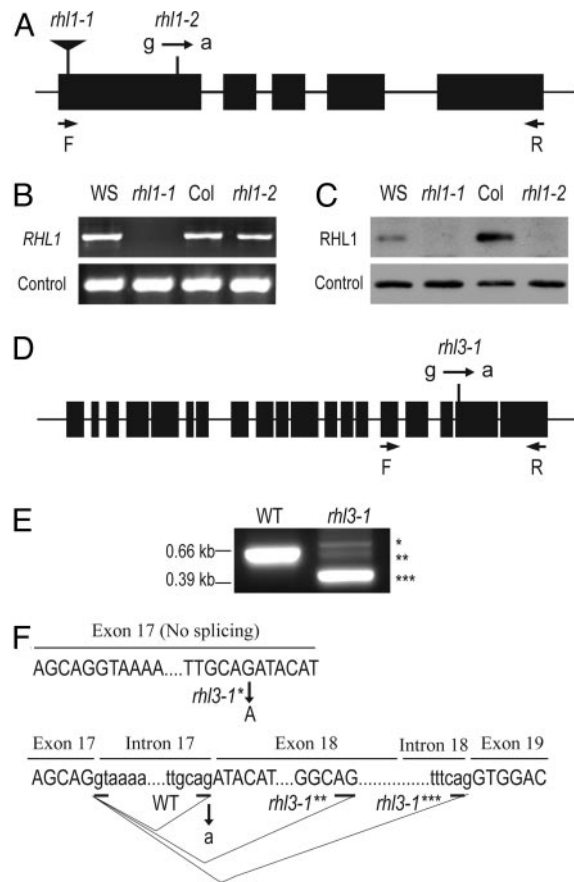


Fig. 3. Positional cloning, transcript, and protein expression analyses of *hyp7* and *rhl3-1*. (A) RHL1 gene structure. The black boxes represent exons. The *rhl1-2* mutation substitutes adenine (a) for guanine (g) in the first exon. (B) RT-PCR analysis of the RHL1 transcript. PCR primers used to amplify the RHL1 transcript are indicated by a pair of arrows. Transcripts of elongation factor 4 were amplified from same RNA sources as the control. (C) Immunoblot analysis of the RHL1 protein. Ten-day-old seedlings of wild-type Wassilewskija ecotype (WS), *rhl1-1*, wild-type Columbia ecotype (Col), and *rhl1-2* were homogenized in SDS buffer and subject to gel electrophoresis. The RHL1 protein was probed with an antiserum raised against the synthetic RHL1 peptide 5KGGDKD-DAESKQRK. (Upper) The signal that corresponds to a size of \approx 39 kDa is absent in *rhl1-1* and *rhl1-2*. (Lower) Antibodies against tubulin were used as a loading control. (D) *AtTOP6B/HYP6/RHL3* gene structure. The *rhl3-1* mutation substitutes adenine (a) for guanine (g) in the 17th intron. (E) RT-PCR analysis of the *AtTOP6B/HYP6/RHL3* transcript. PCR primers indicated by a pair of arrows in D amplified a 0.66-kb fragment from Col and 0.74-, 0.63-, and 0.39-kb fragments (indicated by *, **, and ***, respectively) from *rhl3-1*. (F) A schematic representation of splice products detected in *rhl3-1*. The sequence highlights relevant parts of genomic DNA. Sequences of introns and exons are indicated by lowercase and uppercase letters, respectively. The guanine (g)-to-adenine (a) substitution in *rhl3-1* shown by an arrow abolishes the wild-type splicing acceptor site (ag) of intron 17, which results in the following three aberrant splicing events: to skip splicing intron 17 (*), to splice intron 17 at the next available acceptor site in exon 18 (**), or to splice introns 17 and 18 and exon 18 by using the acceptor site of intron 18 (***)

HYP6 (At3g20780), a plant homologue of archaeal topo VI subunit B. The *rhl3-1* mutant has a single-nucleotide exchange from guanine to adenine at the splicing acceptor site of the 17th intron (Fig. 3D). By using RT-PCR analysis, we found that this mutation abolishes proper splicing of the *AtTOP6B/HYP6* transcript, resulting in the transcription of mRNA with at least three altered sizes (Fig. 3E). All of these misspliced products create a premature stop codon in the following exon (Fig. 3F), suggesting that *rhl3-1* functions as a null allele. The genetic cross between *rhl3-1* and *hyp6*, another mutant allele of *AtTOP6B* (described in

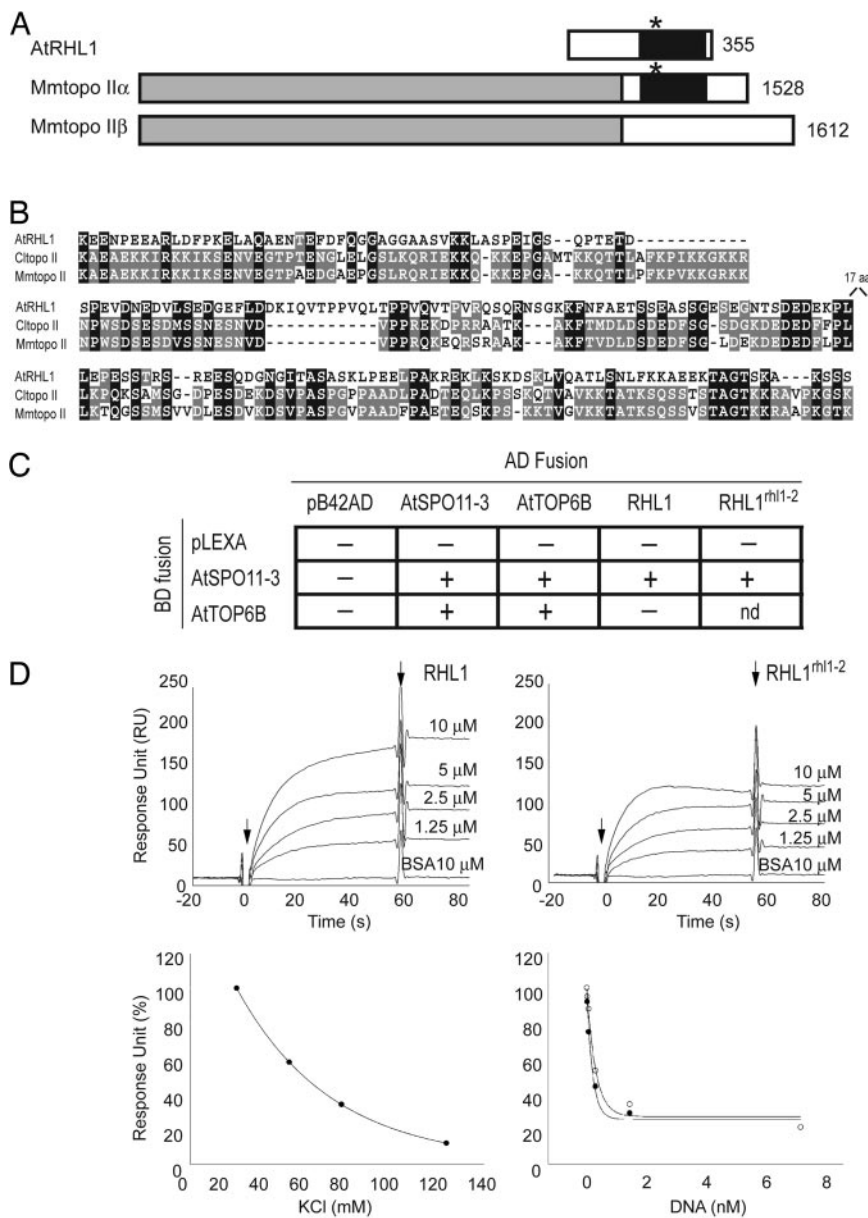


Fig. 4. RHL1 interacts with AtSPO11-3/RHL2 and tightly binds to DNA. (A) Schematic alignment of AtRHL1, mammalian topo II α , and topo II β . Black boxes represent a domain similar between AtRHL1 (RHL1 from *Arabidopsis thaliana*) and Mmtopo II α (topo II α from *Mus musculus*). Gray boxes represent a domain highly ($\approx 78\%$) homologous between Mmtopo II α and Mmtopo II β . Numbers refer to the amino acid length of each deduced protein. Asterisks indicate putative PEST sequences. (B) Multiple sequence alignment of C-terminal domain of AtRHL1, Mmtopo II α , and Cltopo II α [topo II α from hamster (*Cricetulus longicaudatus*)]. Accession numbers used for the analysis are NP564526 (for AtRHL1), NP035753 (for Mmtopo II α), and CAA76313 (for Cltopo II α). (C) *In vivo* interaction of RHL1 with AtSPO11-3/RHL2 detected by yeast two-hybrid analysis. Interaction was assayed by induction (+) or no induction (-) of the *lacZ* reporter gene. nd, not determined. (D) RHL1 binds to DNA *in vitro*. (Upper Left) Biacore SPR sensograms indicate that T7::RHL1 binds to a double-stranded DNA (147 bp) in a concentration-dependent manner. Arrows mark beginning and end of the protein injection. (Upper Right) The DNA binding of T7::RHL1^{rh11-2} is not qualitatively altered. (Lower Left) The DNA binding of RHL1 is salt-dependent (Lower Left) and competed by supercoiled (○) and relaxed (●) pBR322 plasmid DNA (Lower Right). T7::RHL1 (2.5 μ M) was preincubated with various concentrations of supercoiled or relaxed pBR322 plasmid DNA before injection.

ref. 9), does not complement the mutant phenotype, thus confirming the allelism of the two mutations.

RHL1 Interacts with RHL2 *in Vivo*. The RHL1 protein has been described as a plant-specific, nuclear-targeted protein of unknown function (20). Apart from several putative nuclear localization signals, phosphorylation sites and a PEST sequence [a putative proteasome-dependent protein degradation motif (21)], the deduced amino acid sequence of RHL1 (Fig. 4A) does not have strong homology to any functional domains characterized to date. However, by sequence analysis with PHI-BLAST, we found that the C terminus of RHL1 has weak but significant sequence similarity to the C-terminal ≈ 220 aa of mammalian DNA topo II α , sharing, for example, a total of 22% identical and 11% similar amino acids with mouse topo II α (Fig. 4A and B). Eukaryotic topo II belongs to a subclass of type II topo (type IIA) and is required to untangle newly replicated double-stranded DNA during chromosome segregation (22). Only mammalian species, including mouse, hamster, and human, appear to have two isoforms of topo II, topo II α and topo II β , but exactly how their functions differ is not clear. topo II α and

topo II β in mouse are encoded by separate genes to form $\approx 1,530$ - and $\approx 1,620$ -residue proteins, respectively. These share up to 78% sequence homology at their N-terminal three-quarters but only 34% at their C-terminal quarter (23). Our sequence analysis did not detect significant amino acid identities between RHL1 and topo II β (Fig. 4A).

Our findings that the *rh11* phenotype is indistinguishable from that of topo VI mutants *Atspo11-3/rhl2* and *Attop6b/hyp6/rhl3* (Fig. 1D-F) and that RHL1 has sequence similarity to a functionally related topo II α (Fig. 4A and B) suggest that RHL1 functions closely with topo VI. To investigate the functional relationship between RHL1 and topo VI, we generated double mutants between *rh11* and our topo VI mutants. As shown in Fig. 1G and H, both *rh11-2 rh12-1* and *rh11-2 rh13-1* double mutants show a dwarf phenotype nearly identical to that of their respective parents, suggesting that, genetically, RHL1 functions in the same pathway or complex as topo VI. To further test whether RHL1 can form a protein complex with topo VI, we used a yeast two-hybrid assay to examine whether RHL1 interacts with topo VI *in vivo*. Hartung and Puchta (24) previously reported that AtSPO11-3/RHL2 can inter-

act with AtTOP6B/HYP6/RHL3 in a yeast interaction assay. In addition, we found that both proteins also self-interact (Fig. 4C), suggesting that *Arabidopsis* topo VI forms a similar A₂B₂ heterotetramer complex as archaeal topo VI (14). Furthermore, our interaction assay showed that RHL1 can bind to AtSPO11-3/RHL2 but not directly to AtTOP6B/HYP6/RHL3 (Fig. 4C), suggesting that RHL1 forms a protein complex with topo VI by binding to subunit A. By expressing the RHL1^{rhl1-2} protein we found that the *rhl1-2* mutation does not interfere with RHL1 binding to AtSPO11-3/RHL2, at least not in yeast (Fig. 4C).

RHL1 Binds to DNA *in Vitro*. The function of topo II's C-terminal region is not well understood, except that it is implicated in the regulation of topo II (25). Recent studies on two other closely related type IIA topoisomerases, DNA gyrase and topo IV, suggest that their C-terminal domains bind and bend DNA to correctly position substrate DNA for the enzymatic reaction (26, 27). Although RHL1 does not have significant homology to the C terminus of DNA gyrase or topo IV, it is possible that RHL1 performs a similar function. We therefore tested whether the recombinant RHL1 protein can bind to DNA *in vitro* (see *Supporting Materials and Methods* for details). Using surface plasmon resonance (SPR), we found that RHL1 binds to DNA in a concentration- and salt-dependent manner (Fig. 4D). Two of the recombinant proteins tested, T7::RHL1 and His::S::RHL1, but not our His::control protein exhibit similar DNA-binding properties, indicating that the observed DNA binding is not an artifact of fusion tags on their N terminus. In addition, we found that the preincubation of the RHL1 protein with various concentrations of relaxed or negatively supercoiled pBR322 plasmid DNA reduces the affinity of RHL1 for the DNA fragment on the SPR chip (Fig. 4D), providing further evidence for the specific binding of RHL1 to DNA. Relaxed and negatively supercoiled DNAs are equally efficient at reducing the DNA-binding capacity of RHL1 (Fig. 4D), suggesting that DNA binding by RHL1 is insensitive to DNA topology. The DNA binding of RHL1 we measured *in vitro* does not appear to be lost by the *rhl1-2* mutation, although its efficiency might be slightly reduced (Fig. 4D).

Differential Requirement of topo II and topo VI in *Arabidopsis*. Our phenotypic analysis suggests that the plant topo VI complex is required for the endocycle beyond 8C. Plant topo VI appears to be dispensable for the mitotic cell cycle because the mutant callus can proliferate as efficiently as wild-type (Fig. 1 *O* and *P*). The *Arabidopsis* genome encodes a gene for another topo II, and its abundance has been previously correlated with cell proliferation (28). Although topo II and topo VI have distinct primary sequences and tertiary structures, they share a number of enzymatic properties *in vitro* (29). It is therefore possible that topo II can resolve chromosome entanglements during the mitotic cell cycle and early stages of the endocycle. To test this possibility, we first examined the level of topo II and topo VI gene expression in proliferating and endoreduplicating cells. From a recent microarray analysis that clustered gene expression profiles associated with cell cycle transitions in *Arabidopsis* leaves (17), we found that the topo II gene, *AtTOP2*, is preferentially expressed in proliferating cells, whereas all topo VI genes, *AtSPO11-3/RHL2*, *AtTOP6B/HYP6/RHL3*, and *RHL1*, are expressed in proliferating and endoreduplicating cells. Our RT-PCR analysis of *Arabidopsis* leaves harvested at equivalent developmental stages confirmed the differential expression patterns between topo II and topo VI (Fig. 5A). In addition, our *in vivo* visualization revealed that the AtSPO11-3/RHL2 protein fused to GFP is present in both shoot apical meristem and young leaf petiole cells (Fig. 5B), further supporting our finding that the topo VI protein is expressed during the mitotic cell cycle and endocycle. The presence of the GFP signal in a subpopulation of cells suggests that the expression and/or stability of the protein are tightly regulated.

To further address the functional relationship between topo II

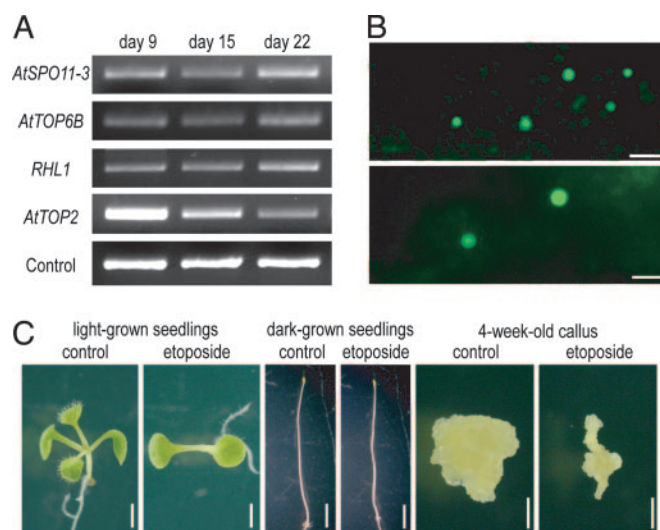


Fig. 5. Functional relationship between topo II and topo VI in *Arabidopsis*. (A) RT-PCR analysis of topo II and topo VI genes. *AtSPO11-3/RHL2*, *AtTOP6B/HYP6/RHL3*, and *RHL1* are expressed more or less equally in proliferating (day 9), endoreduplicating (day 15), and mature (day 22) cells, whereas *AtTOP2* is most strongly expressed in proliferating cells (day 9). The control represents transcripts of an actin gene amplified from the same RNA sources. (B) *In vivo* localization of AtSPO11-3/RHL2::GFP in the shoot apical meristem (Upper) and young leaf petiole (Lower). (C) Plant topo II plays key roles for the mitotic cell cycle but is dispensable for the endocycle. Wild-type seedlings were germinated on plates with 100 μ M etoposide and grown in the light or in the dark for 7 days. Callus was produced from wild-type roots on plates with 100 μ M etoposide. (Scale bars: 10 μ m in B and 2 mm in C.)

and topo VI, we treated wild-type seedlings with a topo II poison, etoposide, at the concentration that blocks the *Arabidopsis* topo II activity *in vitro* (30). As shown in Fig. 5C, seedlings germinated in the light with 100 μ M etoposide are able to expand cotyledons and form short roots but fail to develop true leaves and to establish root systems, strongly suggesting the requirement of topo II for cell proliferation at the shoot and root apical meristems. We also found that etoposide inhibits callus formation severely, further confirming that topo II plays a major role during the mitotic cell cycle (Fig. 5C). *Arabidopsis* hypocotyls elongate primarily by cell expansion in the dark, which is correlated with an increase in the ploidy level through endoreduplication (31). We found that 100 μ M etoposide has little effect on the hypocotyl elongation in the dark (Fig. 5C) or its ploidy level (data not shown), suggesting that topo II is dispensable for endoreduplication. A higher concentration (170 μ M) of etoposide inhibits archaeal topo VI activity *in vitro* (32) but a concentration up to 200 μ M etoposide does not perturb hypocotyl elongation or phenocopy topo VI mutants, suggesting that etoposide does not affect plant topo VI at these concentrations.

Discussion

RHL1, RHL2, and RHL3 Form a Functional Complex Required for Ploidy-Dependent Cell Growth. The three *rhl* mutants were originally identified in a screen for mutants deficient in the formation of root epidermal hair cells (12). This study clearly demonstrates that the primary defects in these mutants are in a more general cell growth control mechanism. We show that GL2, a key player of epidermal cell specification (33), is correctly expressed in *rhl1-2* (Fig. 1), suggesting that RHL1 is not directly involved in the determination of epidermal cell fate. Because the reduced cell size phenotype in *rhl1-2* is associated with its defect in endoreduplication (Fig. 2), RHL1 is likely to have an essential role in ploidy-dependent cell growth in *Arabidopsis*. Endoreduplication is generally thought to provide a mechanism to increase cell size (3), although the corre-

lation between ploidy level and cell size is not always tight (4, 34, 35). In *rhl1-2* leaf epidermis, the maximum DNA content (Fig. 2) and cell size (Fig. 6) are reduced to roughly half the wild-type level, indicating that the *rhl1-2* mutation does not interfere with the linear relationship described for wild-type leaf epidermis (36).

Our genetic and *in vivo* data strongly suggest that RHL1 functions in a plant topo VI complex with AtSPO11-3/RHL2 and AtTOP6B/HYP6/RHL3. Because *rhl1-2* is epistatic to various over-endoreduplicated, over-branched trichome mutants (Fig. 7), the plant topo VI complex appears to be essential in resolving entangled chromosomes during endocycles beyond 8C. At least one component of the topo VI complex, AtSPO11-3/RHL2, appears to be present only transiently *in vivo* (Fig. 5B), implying that topo VI functions at some specific stage (e.g., S phase) of the cell cycle.

It is possible that the plant topo VI complex also functions in other cellular processes because *RHL1*, *AtSPO11-3/RHL2*, and *AtTOP6B/HYP6/RHL3* are expressed from very early to late stages of leaf development (Fig. 5A). The reduced cell number in *rhl1-2* leaves suggests that plant topo VI may participate in the mitotic cell cycle. However, our callus growth results (Fig. 1) show that topo VI is dispensable for cell proliferation *per se*, and our expression analysis and inhibitor study (Fig. 5) suggest that topo II plays a major role during the mitotic cell cycle in plants. It is likely that topo II and topo VI have distinct but partially overlapping functions during the mitotic cell cycle and endocycle.

Role of RHL1 in the Plant topo VI Complex. Because the loss of RHL1 function leads to a phenotype as severe as that of topo VI mutants, it is clear that RHL1 plays an essential role in the plant topo VI complex. In some organisms, topoisomerases are thought to be part of a large protein complex, and some proteins and/or protein complexes may modulate topo activities (37–39). In addition to the work on *Barren* in *Drosophila* (38), this study provides direct genetic evidence that an additional component in the topo complex plays a vital role to modify its function. We have shown that RHL1 can bind to DNA (Fig. 4D), and our competition study indicates that RHL1 has a similar affinity for both supercoiled and relaxed DNA (Fig. 4D). We speculate that this interaction with DNA may have a role in the decatenation reaction of topo VI, e.g., positioning and/or stabilizing substrate DNA. The G79D mutation in *rhl1-2* destabilizes the RHL1 protein *in vivo* (Fig. 3C), which we predict to be the primary cause of the mutant phenotype because recombinant mutated protein retains reasonable DNA binding (Fig. 4D) and interaction with AtSPO11-3/RHL2 (Fig. 4C). However, it should be noted that the lack of interference of the *rhl1-2* mutation is in the context of

the *in vitro* DNA-binding assay and yeast two-hybrid interaction assay and may not represent the *in planta* situation. The nature of RHL1's DNA binding is currently unknown because it does not possess any known DNA-binding motifs found in various transcription factors or other proteins involved in DNA interactions.

This study shows that RHL1 has sequence similarities to the topo II α C-terminal domain. Both topo II and topo VI can decatenate chromosomes but they share very little sequence similarity, except several conserved motifs (29). It is intriguing that these two distantly related enzymes appear to have evolved a similar domain to extend their function. All archaeal genomes that have been fully sequenced to date encode subunits A and B of topo VI but domains homologous to RHL1 have never been identified (P. Forterre, personal communication), indicating that the integration of RHL1 into the topo VI complex did not occur in archaea. Because eukaryotic chromosomes are far larger than the relatively small and simple archaeal chromosomes, it is possible that plant topo VI has acquired a protein partner, such as RHL1, to refine its function.

RHL1's similarity to topo II α and not to topo II β may provide important clues to its function. Although the function of their C-terminal domains is not well understood, the least conserved amino acid sequence between the two isoforms is in this domain and suggests that it may be crucial for their differential regulation (23). Both RHL1 and topo II α C-terminal domains possess several putative phosphorylation sites and the PEST sequence, and these may confer some regulatory roles by modulating subcellular localization or stability of topoisomerases and/or their interaction with other cellular proteins. The C-terminal domain (residues 1207–1528) of mouse topo II α is dispensable for enzymatic activity *in vitro* but is required to complement yeast *top2* mutations (40), supporting the view that RHL1 is not involved in catalysis by topo VI but is required for its regulation.

We thank Herman Hofte (l'Institut National de la Recherche Agronomique, Versailles, France) for providing *hyp7* seeds; Martin Hulskamp for providing *kak*, *try*, and *rfl* seeds; Patrick Forterre for the archaeal genome analysis; Jean-Marc Bonneville for sharing information on *KAK* before publication; Julia Corsar and Daisy Moore for their technical assistance with the genetic analysis of *hyp7*; Ruth Flatman for advice on the SPR analysis; and Sascha Keller (John Innes Centre) for kindly providing a His-tagged control protein for SPR. This work was supported by the Biotechnology and Biological Sciences Research Council of the United Kingdom as a grant (to A.M., K.R., and K.S.-S.) and as a David Phillips Fellowship (to K.S.-S.). K.S.-S. was supported by a Postdoctoral Fellowship for Research Abroad from the Japan Society for the Promotion of Science.

- Jorgensen, P. & Tyers, M. (2004) *Curr. Biol.* **14**, R1014–R1027.
- Conlon, I., Lloyd, A. M., & Raff, M. (2004) in *Cell Growth: Control of Cell Size*, eds. Hall, M. N., Raff, M., & Thomas, G. (Cold Spring Harbor Lab. Press, Plainview, NY), pp. 85–99.
- Sugimoto-Shirasu, K. & Roberts, K. (2003) *Curr. Opin. Plant Biol.* **6**, 544–553.
- Leiva-Neto, J. T., Grafi, G., Sabelli, P. A., Woo, Y. M., Dante, R. A., Maddock, S., Gordon-Kamm, W. J., & Larkins, B. A. (2004) *Plant Cell* **16**, 1854–1869.
- Boudolf, W., Vlieghe, K., Beemster, G. T. S., Magyar, Z., Acosta, J. A. T., Maes, S., Van Der Schueren, E., Inze, D., & De Veylder, L. (2004) *Plant Cell* **16**, 2683–2692.
- Verkest, A., Manes, C. L. D., Vercauteren, S., Maes, S., Van der Schueren, E., Beeckman, T., Genschik, P., Kuiper, M., Inze, D., & De Veylder, L. (2005) *Plant Cell* **17**, 1723–1736.
- Vlieghe, K., Boudolf, W., Beemster, G. T. S., Maes, S., Magyar, Z., Atanassova, A., Engler, J. D., De Groot, R., Inze, D., & De Veylder, L. (2005) *Curr. Biol.* **15**, 59–63.
- Yin, Y. H., Cheong, H., Friedrichsen, D., Zhao, Y. D., Hu, J. P., Mora-Garcia, S., & Chory, J. (2002) *Proc. Natl. Acad. Sci. USA* **99**, 10191–10196.
- Sugimoto-Shirasu, K., Stacey, N. J., Corsar, J., Roberts, K., & McCann, M. C. (2002) *Curr. Biol.* **12**, 1782–1786.
- Hartung, F., Angelis, K. J., Meister, A., Schubert, I., Melzer, M., & Puchta, H. (2002) *Curr. Biol.* **12**, 1787–1791.
- Buhler, C., Gadelle, D., Forterre, P., Wang, J. C., & Bergerat, A. (1998) *Nucleic Acids Res.* **26**, 5157–5162.
- Schneider, K., Wells, B., Dolan, L., & Roberts, K. (1997) *Development (Cambridge, U.K.)* **124**, 1789–1798.
- Hulskamp, M., Misra, S., & Jurgens, G. (1994) *Cell* **76**, 555–566.
- May, M. J., & Leaver, C. J. (1993) *Plant Physiol.* **103**, 621–627.
- Masucci, J. D., Rerie, W. G., Foreman, D. R., Zhang, M., Galway, M. E., Marks, M. D., & Schiefelbein, J. W. (1996) *Development (Cambridge, U.K.)* **122**, 1253–1260.
- Abramoff, M. D., Magelhaes, P. J., & Ram, S. J. (2004) *Biophoton. Int.* **11** (7), 36–42.
- Beemster, G. T., De Veylder, L., Vercauteren, S., West, G., Rombaut, D., Van Hummelen, P., Galichet, A., Gruijssem, W., Inze, D., & Vuytsteke, M. (2005) *Plant Physiol.* **138**, 734–743.
- Clough, S. J., & Bent, A. F. (1998) *Plant J.* **16**, 735–743.
- Perazza, D., Herzog, M., Hulskamp, M., Brown, S., Dorne, A. M., & Bonneville, J. M. (1999) *Genetics* **152**, 461–476.
- Schneider, K., Mathur, J., Boudonck, K., Wells, B., Dolan, L., & Roberts, K. (1998) *Genes Dev.* **12**, 2013–2021.
- Rechsteiner, M., & Rogers, S. W. (1996) *Trends Biochem. Sci.* **21**, 267–271.
- Wang, J. C. (2002) *Nat. Rev. Mol. Cell Biol.* **3**, 430–440.
- Austin, C. A., & Marsh, K. L. (1998) *BioEssays* **20**, 215–226.
- Hartung, F., & Puchta, H. (2001) *Gene* **271**, 81–86.
- Gadelle, D., Filee, J., Buhler, C., & Forterre, P. (2003) *BioEssays* **25**, 232–242.
- Corbett, K. D., Shultzaberger, R. K., & Berger, J. M. (2004) *Proc. Natl. Acad. Sci. USA* **101**, 7293–7298.
- Hsieh, T. J., Farh, L., Huang, W. M., & Chan, N. L. (2004) *J. Biol. Chem.* **279**, 55587–55593.
- Xie, S., & Lam, E. (1994) *Nucleic Acids Res.* **22**, 5729–5736.
- Corbett, K. D., & Berger, J. M. (2004) *Annu. Rev. Biophys. Biomol. Struct.* **33**, 95–118.
- Makarevitch, I., & Somers, D. A. (2005) *Plant Sci.* **168**, 1023–1033.
- Gendreau, E., Traas, J., Desnos, T., Grandjean, O., Caboche, M., & Hofte, H. (1997) *Plant Physiol.* **114**, 295–305.
- Bergerat, A., Gadelle, D., & Forterre, P. (1994) *J. Biol. Chem.* **269**, 27663–27669.
- Schiefelbein, J. (2003) *Curr. Opin. Plant Biol.* **6**, 74–78.
- Gendreau, E., Hofte, H., Grandjean, O., Brown, S., & Traas, J. (1998) *Plant J.* **13**, 221–230.
- Schneidter, A., Weinl, C., Bouyer, D., Schobinger, U., & Hulskamp, M. (2003) *Plant Cell* **15**, 303–315.
- Melaragno, J. E., Mehrotra, B., & Coleman, A. W. (1993) *Plant Cell* **5**, 1661–1668.
- Li, K., Pasternak, C., Hartig, E., Haberezzell, K., Maxwell, A., & Klug, G. (2004) *Nucleic Acids Res.* **32**, 4563–4575.
- Bhat, M. A., Philp, A. V., Glover, D. M., & Bellen, H. J. (1996) *Cell* **87**, 1103–1114.
- Lee, C. G., Hague, L. K., Li, H., & Donnelly, R. (2004) *Cell Cycle* **3**, 638–647.
- Adachi, N., Miyaake, M., Kato, S., Kanamaru, R., Koyama, H., & Kikuchi, A. (1997) *Nucleic Acids Res.* **25**, 3135–3142.